The Colours of Elliptical Galaxies

Ruixiang Chang [1,2], Anna Gallazzi [2], Guinevere Kauffmann[2], Stéphane Charlot[2,3],Željko Ivezić[4], Jarle Brinchmann[5], Timothy M. Heckman[6]

ABSTRACT

We have compiled a sample of 2035 nearby ($z < 0.08$) elliptical galaxies with photometry in the g, r, i, z bands from the Sloan Digital Sky Survey (SDSS) and J, H, K photometry from the Two Micron All Sky Survey (2MASS). Stellar masses, stellar velocity dispersions and structural parameters such as sizes and surface mass densities are also available for these objects. We find that the optical ($g - r$ and $r - i$) and infrared ($J - K$) colours of ellipticals correlate most strongly with their stellar masses and velocity dispersions. In contrast optical-infrared colours ($r - z$, $r - J$, $r - K$) correlate most strongly with their stellar surface mass densities. The correlation of $r - J$ or $r - K$ colour with stellar surface mass density is a factor of two stronger than the corresponding correlations with M_* or σ. This means that optical-infrared colours probe a different aspect of the formation history of ellipticals. We also study the correlations between the stellar absorption line strengths and the colours of the galaxies and we show that optical colours are sensitive to a combination of age, metallicity and α-enhancement. Optical-infrared colours, on the other hand, are sensitive to metallicity and to α-enhancement, but are much less sensitive to age. We speculate that the strong correlation of optical-infrared colours with stellar surface density may reflect the fact that highest density ellipticals formed their stars over the shortest timescales.

1. Introduction

It is well known that the observed properties of elliptical galaxies obey a number of tight relations: the most well-studied of these are the colour-magnitude relation (CMR), the fundamental plane and the Mg-σ relation (see for example Bernardi et al 2003a,b,c,d and references therein). These correlations link the properties of the stellar

[1]Shanghai Astronomical Observatory, 80 Nandan Road, Shanghai, China, 200030

[2]Max Planck Institut fur Astrophysik, D-85748 Garching, Germany

[3]Institut d'Astrophysique du CNRS, 98 bis Boulevard Arago, F-75014 Paris, France

[4]Astronomy Department, University of Washington, Seattle, WA 98195, USA

[5]Centro de Astrofisica da Universidade do Porto, Rua das Estrelas, 4150-762 Porto,Portugal

[6]Department of Physics and Astronomy, Johns Hopkins University, Baltimore, MD 21218 USA

populations of early-type galaxies with their masses and their structural properties and are believed to encode important information about how early-type galaxies formed.

It has long been known that early-type galaxies in nearby clusters exhibit a tight colour-magnitude relation, i.e. more luminous ellipticals have redder colours than less luminous ellipticals (Visvanathan & Sandage 1977; Bower et al. 1992). This work has been extended to moderate redshift and it is found that there is no significant change in the slope with redshift (Aragon-Salamanca et al. 1993; Stanford et al. 1995; 1998; Ellis et al. 1997; Kodama et al. 1998; Holden et al. 2004). The zero-point of the relation shows modest colour evolution, consistent with the passive ageing of a stellar population formed before $z \simeq 2$. Furthermore, the CMR of ellipticals has been found to show little dependence on environment (Terlevich et al. 2001; Bernardi et al. 2003d; Hogg et al. 2004).

The origin of the CMR is still a matter of controversy. The conventional interpretation of the CMR is that it is primarily a metallicity effect (Faber 1977; Dressler 1984; Arimoto & Yoshii 1987; Kodama & Arimoto 1997; Ferreras, Charlot & Silk 1999). It is often assumed that elliptical galaxies form monolithically in a single giant burst of star formation at high redshift. Since the binding energy per unit mass of gas is higher in more massive galaxies, they are able to retain their gas for longer and so reach higher metallicities than less massive galaxies (Larson 1974; Arimoto & Yoshii 1987; Bressan et al 1996; Kodama & Arimoto 1997). Kauffmann & Charlot (1998) and De Lucia et al (2004) have argued that the CMR can also be explained in hierarchical models of galaxy formation when strong feedback is included. In these models, the CMR for elliptical galaxies arises because large ellipticals form by mergers of massive, metal-rich progenitor disk systems. It is, however, also possible to explain at least part of the CMR as an increase in mean stellar age with luminosity (Worthey 1996; Ferreras et al 1999). Indeed, Jorgensen (1999) and Trager et al. (2000) find strong evidence for a significant intermediate-age population in some elliptical galaxies.

Additional information about stellar populations can be gained by studying the strength of stellar absorption features in galaxy spectra. The standard way of quantifying absorption line strengths in galaxies is via the Lick-IDS system, which includes 25 spectral absorption features defined by a 'feature' bandpass and two 'pseudo-continuum' bandpasses. The indices are calibrated using the spectra of 460 Galactic stars over the wavelength range from 4000Å to 6400Å. The sensitivities of different Lick indices to stellar age and metallicity have been discussed in a number of papers (Burstein et al. 1984, Gorgas et al. 1993, Trager et al. 1998, Henry & Worthey 1999). The H-Balmer lines are primarily age-sensitive. Likewise, the 4000Å break (i.e. the ratio of the flux blueward and redward of 4000Å) gets stronger with age, but for old stellar populations, it shows also a second-order sensitivity to metallicity. Indices which are primarily sensitive to metallicity include Fe and Mg lines between 4500Å and 5700Å and molecular features such as the TiO band. In massive elliptical galaxies, the abundance of α-elements with respect to Fe-peak elements can differ from the scaled-solar abundance ratio (Worthey et al. 1992). Indices which trace the abundance of either α-elements or Fe-peak elements can therefore be sensitive to the degree of α-enhancement (Thomas et al. 2003).

In addition to correlations with galaxy luminosity, past studies of elliptical galaxies have also focused on how colours and absorption line indices depend on the stellar velocity dispersion of the galaxy. To first order, both the luminosity and the velocity dispersion of an elliptical are measures of its mass; the luminosity measures the mass contained in stars and the velocity dispersion is a dynamical probe of the total mass contained within some radius. The star formation history of a galaxy, however, may not depend primarily on its mass. Indeed, Kennicutt (1998) has shown that star formation rates in spiral galaxies correlate best with the local surface density of gas and a law of the form $\Sigma_{SFR} = (2.5 \pm 0.7) \times (\frac{\Sigma_{gas}}{1 M_{\odot} pc^{-2}})^{1.4 \pm 0.15} M_{\odot} yr^{-1} kpc^{-2}$ provides a good fit to the data. Bell & De Jong (2000) studied trends in the optical and infrared colours of a sample of nearby spiral galaxies and found that the colours most sensitive to star formation history correlate best with stellar surface density. These results suggest that local rather than global factors regulate the rate at which spiral galaxies form their stars at the present day.

Finally, in a recent work Eisenstein et al (2003) studied how the average optical spectra of massive galaxies in the SDSS vary as a function of both luminosity and environment. They found that as both luminosity and environment change, the variation of pairs of Lick Indices appears to follow a simple one-dimensional locus, suggesting that variations in these two parameters do not lead to independent changes in the spectra of elliptical galaxies.

In this paper, we present the correlations between the colours of elliptical galaxies and a range of different *structural parameters*. We make use of data from the Sloan Digital Sky Survey (SDSS) and the Two Micron All Sky Survey (2MASS) to construct a sample of early-type galaxies with photometry in five optical (u, g, r, i, z) and three near-infrared bands J (1.25μm), H (1.65μm), K_s (2.17μm) bands. Stellar velocity dispersions and size measurements for these systems are available from the SDSS database and estimates of stellar mass are taken from the work of Kauffmann et al (2003a). The outline of the paper is as follows. Section 2 describes how our sample is selected and the method adopted for calculating (K+E)-correction of magnitudes. Section 3.1 presents the the correlations between optical and optical-infrared colours and structural parameters. In section 3.2, we attempt to interpret our results by studying the relations between colours and a variety of Lick indices. Finally, in section 4 we summarize our findings and give our conclusions.

2. The sample

2.1. Properties of the sample

The SDSS is an imaging and spectroscopic survey of the high Galactic latitude sky visible from the Northern hemisphere, which will obtain u, g, r, i and z photometry of almost a quarter of the sky and spectra of at least 700,000 objects (York et al. 2000). A description of the software and data products are given in Stoughton et al. (2002) and Abazajian et al. (2003; 2004). The 2MASS is a ground-based, near-infrared imaging survey of the whole sky and its extended source catalog (XSC) contains almost 1.6 million galaxies (Jarrett et al. 2000a; 2000b). We positionally match sources observed by the 2MASS to galaxies in the 'main' spectroscopic sample of the SDSS Data Release One (DR1; Abazaijan et al. 2003). Galaxies in this sample have $14.5 < r < 17.77$. Practically all 2MASS sources in the DR1 area ($\sim 97\%$ for extended sources from the XSC) are matched to an SDSS counterpart within 2 arcsec. We restrict our analysis to a narrow range of redshift $0.02 < z < 0.08$ in order to minimize uncertainties introduced by K-corrections. The entire matched sample contains 8166 galaxies in this range of redshifts.

In this paper, we focus on early-type galaxies. To select these systems, we require that they have 4000 Å break strength greater than 1.6 (we adopt the narrow definition of the break given in Balogh et al 2001) and concentration parameter $C = R_{90,r}/R_{50,r} > 2.6$ (where $R_{90,r}$ and $R_{50,r}$ are the radii enclosing 90% and 50% of the total Petrosian light of the galaxy). Kauffmann et al (2003b) have shown that this cut separates massive, dense, early-type galaxies from low mass, low density late-type systems. In order to exclude systems with ongoing star formation or residual AGN activity, we also eliminate all galaxies where the equivalent width of the Hα emission line is greater than 2 Å . Finally, we only consider galaxies which have small photometric errors in the near-IR bands; our analysis only includes those ellipticals where the observed errors in $r - J$ are smaller than 0.07. Our final sample contains 2035 early-type galaxies down to a J-band limiting magnitude of about 13.6. Figure 1 shows histograms of the basic properties of the galaxies in our sample. As can be seen, the median redshift of the galaxies in our sample is around 0.05 and their absolute magnitudes lie in the range $-22 < M(r) < -20$.

Stellar mass estimates for this sample are available from the work of Kauffmann et al (2003a). To estimate stellar masses, two stellar absorption line indices, the 4000Å break strength $D_n(4000)$ and the Balmer absorption line index Hδ_A, are used to constrain the mean stellar age of a galaxy and the fraction of its stellar mass formed in bursts over the past few Gyr. A comparison with broad band magnitudes then yields estimates of dust attenuation and of stellar mass. The optical photometric quantities, such as Petrosian magnitudes in 5 bands, size $R_{50,z}$, concentration parameter $C = R_{90,r}/R_{50,r}$, are obtained from the First Data Release (DR1) of the SDSS (Abazajian et al. 2003). It should be noted that all SDSS magnitudes quoted in this paper are Petrosian magnitudes. Velocity dispersion measurements for each galaxy are also available from the database and are described in Schlegel et al (in preparation).

Conversions from apparent magnitude m to absolute magnitude M depend on cosmology and the (K+E)-correction:

$$M = m - 5\log[D_L(z, \Omega_M, \Omega_\Lambda)] - 25 - K(z), \tag{1}$$

where D_L is the luminosity distance in Mpc and $K(z)$ is the sum of K-correction and E-correction for the band, which are described in detail in the next subsection. We assume a cosmology with $\Omega_M = 0.3$, $\Omega_\Lambda = 0.7$ and H_0=70 km s^{-1} Mpc^{-1}.

2.2. (K+E)-correction

When converting from the apparent magnitude to the rest-frame absolute magnitude of an object, the fact that the SDSS and 2MASS filters measure the light from a fixed spectral range in the local frame needs to be taken into account. Correcting for this effect is known as the K-correction. The E-correction accounts for the change in the galaxy's luminosity between the time that its light was emitted and the present day. In this paper, the sum of K-correction and E-correction is denoted as the (K+E)-correction.

In order to evaluate these corrections, we generate a grid of model spectral energy distributions (SEDs) using the population synthesis models of Bruzual & Charlot (2003, BC03). We adopt the universal initial mass function from Chabrier (2003) and lower and upper mass cut-offs are taken as m_L=0.1M$_\odot$ and m_U=100M$_\odot$, respectively. We parameterize the models according to a metallicity Z and the star formation timescale τ. Galaxies form stars according to the equation

$$\Psi(t) = \tau^{-1} e^{-t/\tau}, \tag{2}$$

for a total duration of 12 Gyr. The effect of extinction on the SEDs is not included, because the dust attenuation measurements of Kauffmann et al (2003a) show that there is very little dust in these systems. For each model, we store observer frame colours at a series of closely spaced redshifts from z=0.08 to z=0.02. For each galaxy in our sample, we find the model that most closely reproduces its observed $r - i$ and $r - J$ colours and we use the model to transform to colours and magnitudes defined at z=0.04. Because of the very limited range of redshifts of the galaxies in our sample, these colour corrections are small: 0.04 mag for $g - r$, 0.01 mag for $r - i$ and $r - z$, 0.03 mag for $r - J$ and 0.05 mag for $r - K$ on average.

3. Main Results

3.1. Relations between colours and structural parameters

In this section, we present the correlations of both the optical and the optical-infrared colours of the ellipticals in our sample with the following parameters:

1. absolute r-band magnitude M_r.
2. stellar mass M_*.
3. measured stellar velocity dispersion σ.
4. "inferred" stellar velocity dispersion : $\sigma_{inf} = C(GM_*/R_{50,z})^{1/2}$, where C was chosen so that the average value of σ_{inf} for all the galaxies in the sample would be equal to the average value of σ for the same set of galaxies (we find $C = 0.5$).
5. stellar surface density $\mu_* = 0.5M_*/(\pi R^2_{50,z})$
6. stellar "density" $\rho_* = 0.5M_*/(4/3\pi R^3_{50,z})$

where $R_{50,z}$ is the radius enclosing 50 percent of Petrosian flux in z band (and hence 50 percent of the stellar mass). [7] In this paper, the parameters M_*, σ, σ_{inf}, μ_*, ρ_* are in units of $M_\odot$, km/s, km/s, $M_\odot$/kpc^2 and $M_\odot$/kpc^3, respectively. The results are presented in Figures 2-4, where we show the correlations between $g-r$, $r-i$, $r-J$ and $J-K$ colours as a function of these parameters. We find that a simple least-squares fit to the data in sensitive to whether or not we exclude galaxies that lie far away from the main relations . We thus switched to robust techniques and we fit a straight line to the data using the criterion of least absolute deviations. This is shown as a solid line on the plots.

Table 1 lists the parameters of the fits. The first set of quantities are the best-fit slopes. The second set of quantities *disp* give the dispersions about the relation, which we define as $\sum_{i=1}^{n} \frac{|y_i^o - y_i^m|}{n}$, where y_i^o is the observed colour and y_i^m is the colour predicted by the fit and n is the number of galaxies. The third and fourth set of quantities ΔC measure the changes in colour over the interval in magnitude, mass, σ or density that contains 90% of the galaxies (we exclude the lower and upper 5th percentiles of the distribution). In order to compare these colour changes between different photometric bands, we normalize ΔC by dividing either by the dispersion (set 3) or by the total range in colour enclosing 90% of the galaxies (set 4).

We find a weak correlation between the $g-r$ and $r-i$ optical colours and r-band absolute magnitude. Our results are consistent with those found by Bernardi et al (2003d, see figure 7 in their paper). Table 1 shows that the optical colours correlate more strongly with stellar mass than with r-band magnitude and that the dispersion about the relation is also smaller. In general, the strongest correlation and the smallest

---

[7] We also tried different measurements of z-band half-light radius including the seeing deconvolved Sersic and Petrosian half-light radii derived by Blanton et al (2003). We obtained almost identical results.

dispersion is obtained for the velocity dispersion σ. (Note that M_* scaled by $R_{50,z}$ yields very similar results to σ itself.) The slope that we derive for the $(r-i)-\log\sigma$ relation is consistent with the results of Bernardi et al (2003d), but we obtain a slightly shallower slope for the $(g-r)-\log\sigma$ relation. This is may be because we use the Petrosian magnitudes to evaluate the colours, while they adopted model magnitudes. The correlation of $g-r$ and $r-i$ colours with surface mass density μ_* or with density ρ_* is substantially weaker than the correlation with σ. These results suggest that the optical colour of a galaxy is primarily driven by the *mass* of the system.

Turning to optical-infrared colours, the two measures of correlation strength listed in Table 1 ($\Delta I/disp$ and $\Delta I/range$) shows that the $r-z$ colours of ellipticals exhibit weaker correlations with r-band magnitude and stellar mass and stronger correlations with surface mass density μ_* than do $g-r$ or $r-i$ colours. Figure 3 demonstrates that this trend continues for the SDSS/2MASS optical-infrared colours. There is an *inverse* correlation between $r-J$ colour and absolute magnitude and the correlations of $r-J$ and $r-K$ colours with both stellar mass and velocity dispersion are substantially weaker than their correlations with stellar surface mass density. Interestingly, the strong correlation between colour and surface mass density does not hold for the infrared $J-K$ colour. The $J-K$ colours of the ellipticals in our samples exhibit very similar trends to the $g-r$ or $r-i$ optical colours; the strongest correlations are with stellar mass and velocity dispersion and not with μ_*.

In short, our results indicate that the optical and infrared colours of elliptical galaxies correlate most strongly with velocity dispersion, while optical-infrared colours correlate most strongly with surface mass density.

3.1.1. An investigation of aperture mismatch

In this paper, measurements of the optical (g,r,i,z) magnitudes were obtained from the Sloan Digital Sky Survey database, but the near-infrared data was taken from the Two Micron All Sky Survey. It is thus important to consider whether the different methods for measuring magnitudes employed by SDSS and 2MASS could be leading to systematic effects in our analysis. For example, there might be effects due to the mismatch in angular resolution of the two surveys. This might lead to spurious correlations between SDSS-2MASS colours and the apparent sizes (and hence surface mass densities) of the galaxies.

We tested for this effect by dividing our sample onto a set of galaxy pairs. Each pair was constructed to have stellar masses closer than 0.1 dex in $\log M_*$, 0.1 dex in $\log\mu_*$ and 20 km s^{-1} in velocity dispersion. There are 409 such pairs, i.e. 40% of all the galaxies in our sample are included in this analysis. In Figure 6, we plot the colour difference between the galaxies in each pair as a function of the difference in apparent size. We find no correlation between colour and angular size differences for the SDSS bands. Note that we have plotted K-corrected colours throughout, so this figure also tests the robustness of these corrections (the angular size difference scales with redshift difference in this plot).

On the other hand, we find that the SDSS-2MASS colours do exhibit a significant correlation in the sense that galaxies that are more extended on the sky have bluer optical-infrared colours. This effect produces colour differences of up to 0.2 mag in r-J between the largest and the smallest ellipticals in our sample.

We now test the impact of these aperture mismatches on our results by dividing our sample into narrow bins in apparent size. Figure 7 compares the relation between r-J colour and surface mass density for three different bins in half light radius R50. The solid line shows the fit to the entire sample. As can be seen, as the apparent size increases, galaxies become systematically bluer in $r-J$, but the *slope* of the relation between $r-J$ and $\log\mu_*$ does not appear to change. We find very similar results for the correlation between $r-J$ and other parameters such as stellar mass and velocity dispersion. We thus conclude that aperture mismatch between the SDSS and 2MASS is a source of additional *scatter* in the relations between optical-infrared colour and galaxy parameters. It is not the origin of the strong correlation between optical-infrared colours and stellar surface mass density seen in the data. The fact that we see a smooth transition in the linear fit parameters given in Table 1 as we progress from $r-i$, through $r-z$ to $r-J$ and $r-K$ also gives us confidence that our basic results are robust.

3.2. Stellar absorption features

Studying the relations between stellar absorption features, colours and structural parameters may help us to better understand the physical origin of the results discussed above.

We have measured Lick indices for all the galaxies in the sample from the SDSS spectra, using the bandpass definition of Worthey & Ottaviani (1997). It should be noted that the strengths of some of the absorption indices are strongly affected by broadening due to the velocity dispersion σ of the stars in the galaxy. Indices measured with the narrowest 'pseudo-continuum' bandpasses show the strongest dependence on σ. One approach for dealing with this effect would be to artificially broaden the spectra of the galaxies with low velocity dispersions so that we have the same effective σ for all the galaxies in the sample. However, this leads to significant loss of information. Instead, we study how absorption line indices correlate with colour at a fixed value of σ. We first fit a linear relation between index strength and σ and then we study whether the residuals (ΔI) correlate with galaxy colour.

In Table 2 we summarize the results for a variety of different Lick indices and for $g-r$ and $r-J$ colours. As discussed by Thomas et al (2003), the α-element to Fe abundance ratio can be empirically quantified by the ratio between Mg and Fe indices. Here we use the index ratio $Mg_2/\langle Fe \rangle$. [8] It is also possible to define other combinations of indices that are almost independent of α-enhancement. Those investigated here are [MgFe]$'$, as defined by Thomas et al. 2003, and [Mg_1Fe] and [Mg_2Fe], as given by BC03. For each index, we list the slope of the relation between ΔI and colour (columns 3 and 6) as well as the mean absolute deviation about the relation (columns 4 and 7). The significance of the relation according to a Spearman rank-order test is given in columns 5 and 8. We also provide information about the indices, including the mean signal-to-noise ratio of the index (column 2), the elements that are expected to contribute most to the index strength (column 9) and the sensitivity of the index to α/Fe ratio (column 10). This information was taken from Henry & Worthey (1999) and Thomas et al. (2003).

In Table 2, the quantities of most interest are the *relative* strengths of the correlations between ΔI and colour for different indices. For $g - r$, the strongest correlations are found for three Balmer absorption lines (Hβ, Hγ and Hδ), the 4000 Å break strength $D_n(4000)$, Mg-lines and the α-enhancement independent indices [MgFe]$'$ and [Mg_2Fe]. Other significant, though weaker, correlations are found for some iron lines (Fe4383, Fe5270 and Fe5782), the G-band and C_2. Turning to $r - J$ colours, the main difference we find is that the correlations are much weaker for the three Balmer lines. Significant correlations are still found for the Mg-lines, Fe5270, [MgFe]$'$ and [Mg_2Fe]. The NaD index also exhibits a strong residual correlation with both colours.

Table 3 shows how the residuals correlate with stellar velocity dispersion μ_* rather than colour. Recall that in section 3.1 we showed that $r - J$ colour correlates more strongly with μ_* than with M_* or σ. From Table 3, we see that the strongest correlations of index residuals with μ_* are for metallicity-sensitive indices such as Mgb, Fe4383, C_2 and [MgFe]$'$. Surface mass density does not correlate significantly with the Balmer absorption lines. These results are at least qualitatively consistent with the results in Table 2.

The main conclusion of this analysis, therefore, is that optical colours are probably sensitive to a combination of age, metallicity and α-enhancement, whereas optical-infrared colours are much less sensitive to age and are likely affected by some combination of metallicity and α-enhancement. One caveat that should be mentioned is that the colours are measured for the galaxy as a whole, but that the Lick indices are measured within the 3 arcsecond fiber apertures. Gradients in index strength in our sample of ellipticals might have significant effect on the analysis presented in this section. We have checked whether our results change if we use SDSS "fiber" colours (calculated within a 2.5 arcsec aperture) rather than the Petrosian colours. There are changes in the strengths of some of the correlations, but our main qualitative

[8] The $\langle Fe \rangle$ is the average of Fe5270 and Fe5335 index strengths.

conclusions remain unchanged. We are of course unable to perform the same test for the optical-infrared colours.

4. Discussion

The main aim of this paper is to investigate what can be learned from the optical, infrared and optical-infrared colours of elliptical galaxies. We have put together a sample of ellipticals from a matched sample of galaxies with photometry from both SDSS and 2MASS and spectroscopy from SDSS. We study the correlations between colours and a variety of different parameters. We find that:

1. Luminous and massive elliptical galaxies have redder optical and infrared colours than less luminous and lower mass ellipticals. The optical-infrared colours of ellipticals, on the other hand, exhibit almost no dependence on luminosity or on stellar mass.
2. The optical and infrared colours of elliptical galaxies correlate more strongly with stellar mass than with r-band absolute magnitude. The colour-M_* relation also has smaller dispersion. This suggests that the stellar mass is a more fundamental quantity than r-band luminosity.
3. The optical and infrared colours of ellipticals are most strongly correlated with their velocity dispersions. The optical-infrared colours, on the other hand, are most strongly correlated with their stellar surface mass densities.

Our results show that the optical-infrared colours of elliptical galaxies must be controlled by different physics. This conclusion is confirmed when we study the correlations of a variety of Lick indices with galaxy colour. At fixed stellar velocity dispersion, we find that both metallicity-sensitive and age-sensitive indices exhibit residual correlations with $g - r$, but only metallicity-sensitive indices have residual correlations with $r - J$.

Because optical and infrared colours correlate most strongly with stellar mass and velocity dispersion, it is natural to suppose that more massive ellipticals may have redder colours because they are both older and more metal rich. As discussed by Kodama et al (1998), if the colour-magnitude relation of ellipticals is driven only by stellar age, with low mass ellipticals significantly younger than high mass ellipticals, one would expect the slope of the colour-magnitude or colour-σ to steepen substantially at higher redshift. The slope of the CMR is observed to be constant out to $z \sim 1$ and this can be used as a constraint on the age differences between ellipticals of different mass.

On the other hand, the optical-infrared colours of ellipticals exhibit weak correlations with mass, velocity dispersion and age and strong correlations with stellar surface mass density. The most straightforward interpretation of this result is that optical-infrared colours are sensitive not only to metallicity, but also to α-enhancement. The degree of α-enhancement is a measure of the timescale over which star formation occurred in the elliptical. Tremonti et al (2004) showed that there is a strong correlation between stellar mass and metallicity for emission-line galaxies in the SDSS. Bell & de Jong (2000) and Kauffmann et al. (2003b) found that the star formation histories of disk galaxies as traced by stellar absorption line indices such as the 4000 Å break and Balmer absorption lines, are more fundamentally related to surface mass density than to stellar mass. If these conclusions also extend to ellipticals, then this may provide a natural explanation for the results presented in this paper.

A.G. and S.C. thank the Alexander von Humboldt Foundation, the Federal Ministry of Education and Research, and the Programme for Investment in the Future (ZIP) of the German Government for their support.

Ruixiang Chang acknowledges the financial support of MPG for a visit to MPA and expresses her gratitude for the hospitality during her visit at MPA. This project is partly supported by NSFC 10173017, 10403008, 10133020, 10073016, NKBRSF 1999075404, Shanghai Municipal Science and Technology Commission No. 04dz05905.

Funding for the creation and distribution of the SDSS Archive has been provided by the Alfred P. Sloan Foundation, the Participating Institutions, the National Aeronautics and Space Administration, the National Science Foundation, the U.S. Department of Energy, the Japanese Monbukagakusho, and the Max Planck Society. The SDSS Web site is http://www.sdss.org/.

The SDSS is managed by the Astrophysical Research Consortium (ARC) for the Participating Institutions. The Participating Institutions are The University of Chicago, Fermilab, the Institute for Advanced Study, the Japan Participation Group, The Johns Hopkins University, Los Alamos National Laboratory, the Max-Planck-Institute for Astronomy (MPIA), the Max-Planck-Institute for Astrophysics (MPA), New Mexico State University, University of Pittsburgh, Princeton University, the United States Naval Observatory, and the University of Washington.

REFERENCES

Abazajian K., et al., 2003, AJ, 126, 2018 (DR1 paper)

Abazajian K., et al., 2004, AJ, 128,502

Aragon-Salamanca A., Ellis R.S., Couch W.J. & Carter D., 1993, MNRAS 262, 764

Arimoto N. & Yoshii Y., 1987, A&A 173, 23

Balogh M.L., Christlein D., Zabludoff A.I., Zaritsky D., 2001, ApJ 557, 117

Bell E.F. & de Jong R.S., 2000, MNRAS 312, 497

Bernardi M., Sheth R., Annis J., et al., 2003a, AJ 125, 1817

Bernardi M., Sheth R., Annis J., et al., 2003b, AJ 125, 1849

Bernardi M., Sheth R., Annis J., et al., 2003c, AJ 125, 1866

Bernardi M., Sheth R., Annis J., et al., 2003d, AJ 125, 1882

Blanton M., Hogg D., Bahcall N., et al., 2003, ApJ 594, 186

Bower R.G., Laycey J.R., & Ellis R.S., 1992, MNRAS 254, 601

Bressan A., Chiosi C. & Tantalo R., 1996, A&A 311, 425

Bruzual G. & Charlot S., 2003, MNRAS 344, 1000

Burstein D., Faber S. M., Gaskell C. M., Krumm N., 1984, ApJ, 287, 586

Chabrier G., 2003, PASP 115, 763

De Lucia G., Kauffmann G. & White S.D.M., 2004, MNRAS 349, 1101

Dressler A., 1984, ApJ 286, 97

Eisenstein,D.J., et al, 2003, ApJ 585, 694

Ellis R.S., Smail I., Dressler A., et al., 1997, ApJ 483, 582

Faber S.M., 1977, in Tinsley B.M., Larson R.B., eds, The Evolution of Galaxies and Stellar Populations. Yale Observatory, New Haven, p.157

Ferreras, I., Charlot, S., Silk, J., 1999, ApJ 521, 81

Gorgas J., Faber S. M., Burstein D., Gonzalez J. J., Courteau S., Prosser C., 1993, ApJS, 86, 153

Henry R. B. C., Worthey G., 1999, PASP, 111, 919

Hogg D., Blanton M., Brinchmann J., et al., 2004, ApJ 601, L29

Holden B.P., Stanford S.A., Eisenhardt P. & Dickinson M., 2004, AJ 127, 2484

Jarrett T.J., Chester T., Cutri R., et al., 2000a, AJ 119, 2498

Jarrett T.J., Chester T., Cutri R., et al., 2000b, AJ 120, 298

Jorgensen I., 1999, MNRAS 306, 607

Kauffmann G. & Charlot S., 1998, MNRAS 294, 705

Kauffmann G., Heckman T., White S.D.M., et al., 2003a, MNRAS 341, 33

Kauffmann G., Heckman T., White S.D.M., et al., 2003b, MNRAS 341, 54

Kennicutt R.C., 1998, ApJ 498, 541

Kodama T., Arimoto N., 1997, A&A 320,41

Kodama T., Arimoto N., Barger A. & Aragon-Salamanca A., 1998, A&A 334, 99

Larson R.B., 1974, MNRAS 166, 585

Stanford S.A., Eisenhardt P.R.M. & Dickinson M., 1995, ApJ 450, 512

Stanford S.A., Eisenhardt P.R.M. & Dickinson M., 1998, ApJ 492, 461

Stoughton C., et al., 2002, AJ 123, 485 (EDR paper)

Terlevich A.I., Caldwell N. & Bpwer R.G., 2001, MNRAS 326, 1547

Thomas D., Maraston C., Bender R., 2003, MNRAS, 339, 897

Trager S. C., Worthey G., Faber S. M., Burstein D., Gonzalez J. J., 1998, ApJS, 116, 1

Trager S., Faber S., Worthey G. & Gonzalez J., 2000, AJ 119, 1645

Tremonti C., Heckman T., Kauffmann G., et al., 2004, ApJ, 613, 898

Visvanathan N. & Sandage A., 1977, ApJ 216, 214

Worthey G., Faber S. M., Gonzalez J. J., 1992, ApJ, 398, 69

Worthey G., 1996, in Buzzoni A., Renzini A., eds, ASP Conf. Ser. Vol.86, Fresh Views on Elliptical Galaxies, Astron. Soc. Pac., San Francisco, p.203

Worthey G., Ottaviani D. L., 1997, ApJS, 111, 377

York D., et al., 2000, AJ 120, 1579

This preprint was prepared with the AAS LaTeX macros v4.0.

Table 1: The results of linear fits. The first set of quantities are the best-fit slopes. The second set of quantities *disp* give the dispersions about the relation, which we define as $\sum_{i=1}^{n} \frac{|y_i^o - y_i^m|}{n}$, where y_i^o is the observed colour and y_i^m is the colour predicted by the fit and n is the number of galaxies. The third and fourth set of quantities ΔC measure the changes in colour over the interval in magnitude, mass, σ or density that contains 90% of the galaxies (we exclude the lower and upper 5th percentiles of the distribution). ΔC are normalized by dividing either by the dispersion (set 3) or by the total range in colour enclosing 90% of the galaxies (set 4).

	M_r	$\log(M_*)$	$\log(\sigma)$	$\log(\sigma_{inf})$	$\log(\mu_*)$	$\log(\rho_*)$
slope (g-r)	-0.0123	0.0427	0.1575	0.1500	0.0576	0.0186
slope (r-i)	-0.0094	0.0329	0.1004	0.1064	0.0367	0.0096
slope (r-z)	-0.0056	0.0488	0.1883	0.1940	0.1051	0.0502
slope (r-J)	0.0379	0.0091	0.2563	0.3080	0.3626	0.2385
slope (r-K)	-0.0016	0.0850	0.4470	0.5686	0.4040	0.2281
slope (J-K)	-0.0320	0.0733	0.1601	0.2055	0.0355	-0.0069
disp (g-r)	0.0404	0.0389	0.0371	0.0381	0.0395	0.0409
disp (r-i)	0.0360	0.0346	0.0340	0.0341	0.0355	0.0479
disp (r-z)	0.0499	0.0479	0.0460	0.0459	0.0459	0.0483
disp (r-J)	0.1150	0.1168	0.1142	0.1123	0.0968	0.0968
disp (r-K)	0.1421	0.1398	0.1345	0.1318	0.1214	0.1278
disp (J-K)	0.0707	0.0700	0.0706	0.0706	0.0724	0.0726
$\frac{\Delta I}{disp}(g-r)$	0.6559	1.2237	1.6685	1.4724	1.0886	0.4914
$\frac{\Delta I}{disp}(r-i)$	0.5639	1.0405	1.1618	1.1672	0.7718	0.2171
$\frac{\Delta I}{disp}(r-z)$	0.2405	1.1127	1.6109	1.5795	1.7102	1.1263
$\frac{\Delta I}{disp}(r-J)$	-0.7087	0.0856	0.8827	1.0258	2.7986	2.6674
$\frac{\Delta I}{disp}(r-K)$	0.0232	0.6645	1.3071	1.6131	2.4860	1.9327
$\frac{\Delta I}{disp}(J-K)$	0.9742	1.1446	0.8921	1.0879	0.3669	0.1034
$\frac{\Delta I}{range}(g-r)$	0.1667	0.2939	0.3893	0.3528	0.2704	0.1264
$\frac{\Delta I}{range}(r-i)$	0.2031	0.3620	0.3953	0.3981	0.2742	0.1041
$\frac{\Delta I}{range}(r-z)$	0.0585	0.2600	0.3615	0.3537	0.3829	0.2654
$\frac{\Delta I}{range}(r-J)$	-0.1701	0.0209	0.2104	0.2405	0.5656	0.5390
$\frac{\Delta I}{range}(r-K)$	0.0054	0.1523	0.2882	0.3485	0.4948	0.4049
$\frac{\Delta I}{range}(J-K)$	0.2206	0.2567	0.2019	0.2461	0.0851	0.0241

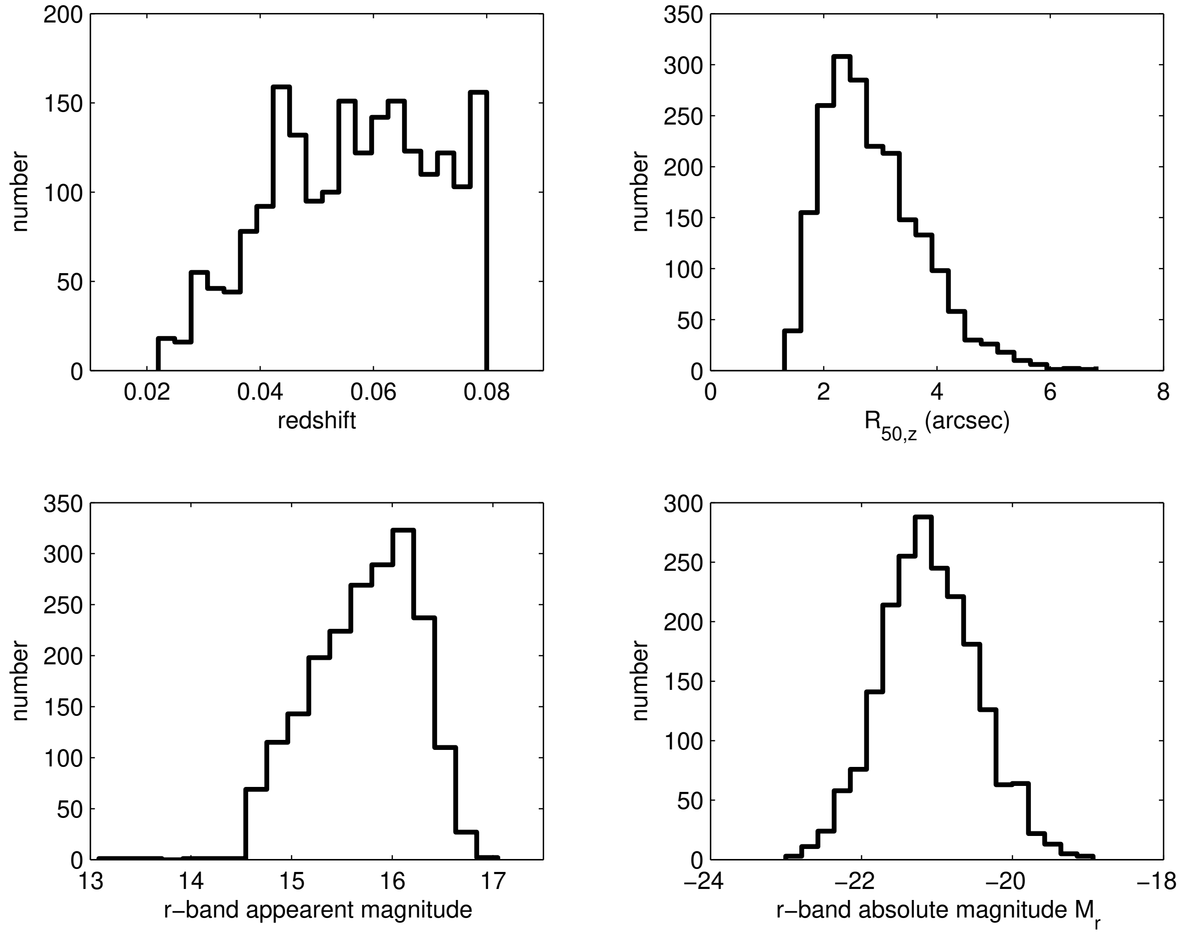

Fig. 1.— The distribution of the redshifts, sizes and magnitudes of the ellipticals in our sample.

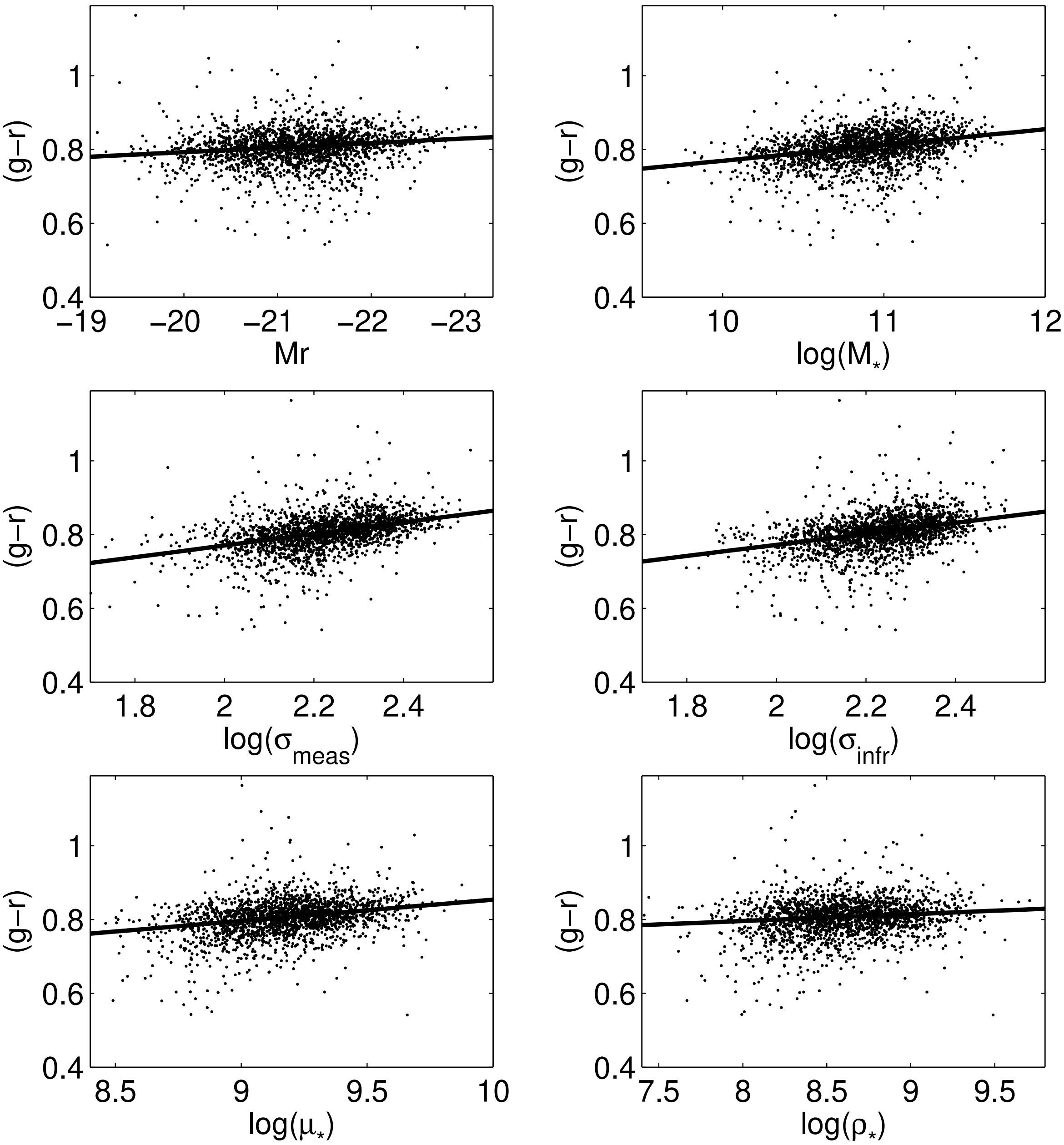

Fig. 2.— The correlations between $g-r$ and r-band magnitude M_r, stellar mass M_* (in units of $\mathrm{M}_\odot$), measured stellar velocity dispersion σ_{meas} (in units of km/s), "inferred" stellar velocity dispersion $\sigma_{inf} = 0.5(GM_*/R_{50,z})^{1/2}$ (in units of km/s), stellar surface mass density $\mu_* = 0.5M_*/(\pi R^2_{50,z})$ (in unit of $\mathrm{M}_\odot/\mathrm{kpc}^2$) and density $\rho_* = 0.5M_*/(4/3\pi R^3_{50,z})$ (in units of $\mathrm{M}_\odot/\mathrm{kpc}^3$). The solid lines show linear fits using robust techniques.

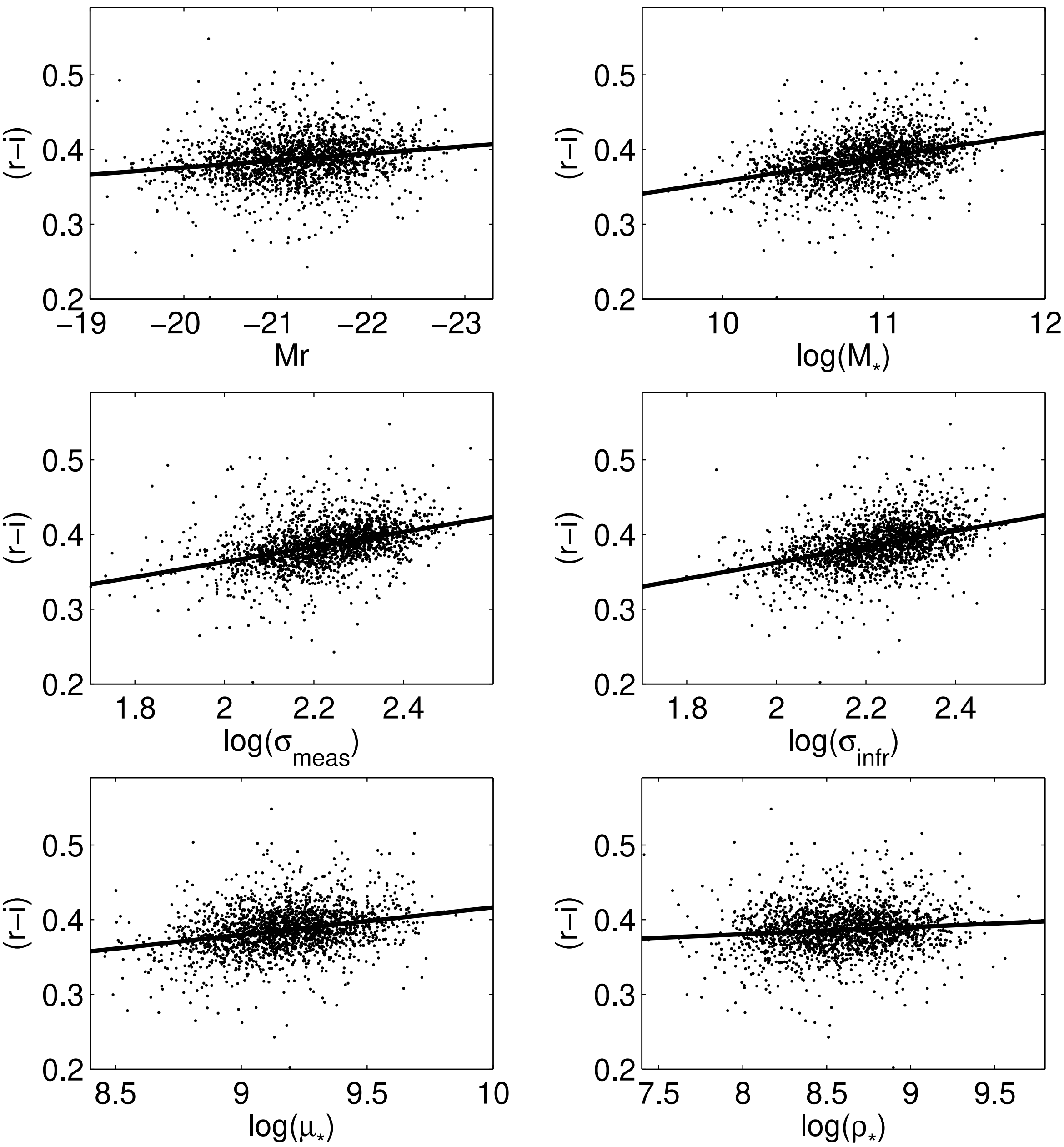

Fig. 3.— Same as figure 2, but for $r - i$ colour.

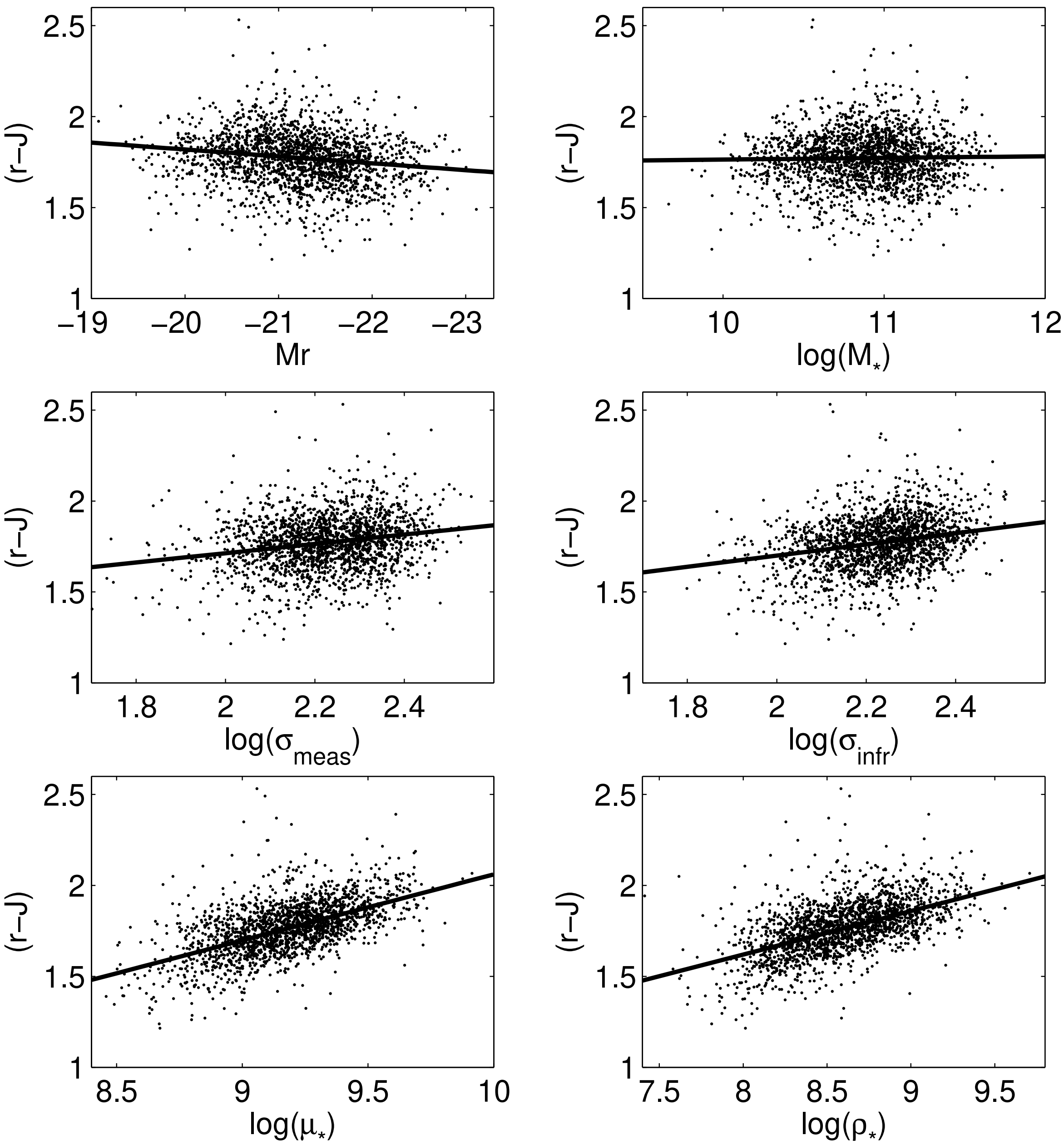

Fig. 4.— Same as figure 2, but for $r - J$ colour.

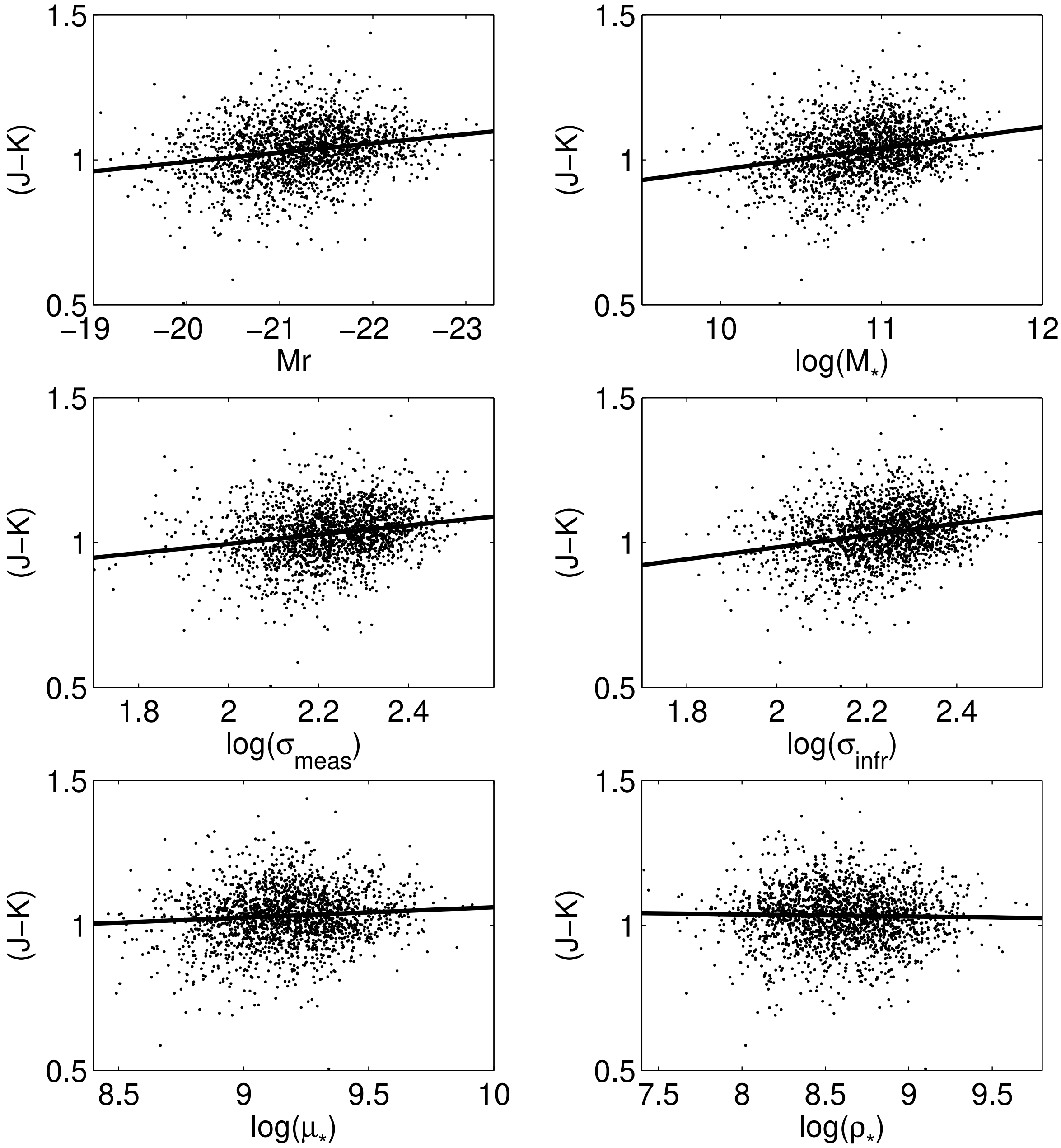

Fig. 5.— Same as figure 2, but for $J - K$ colour.

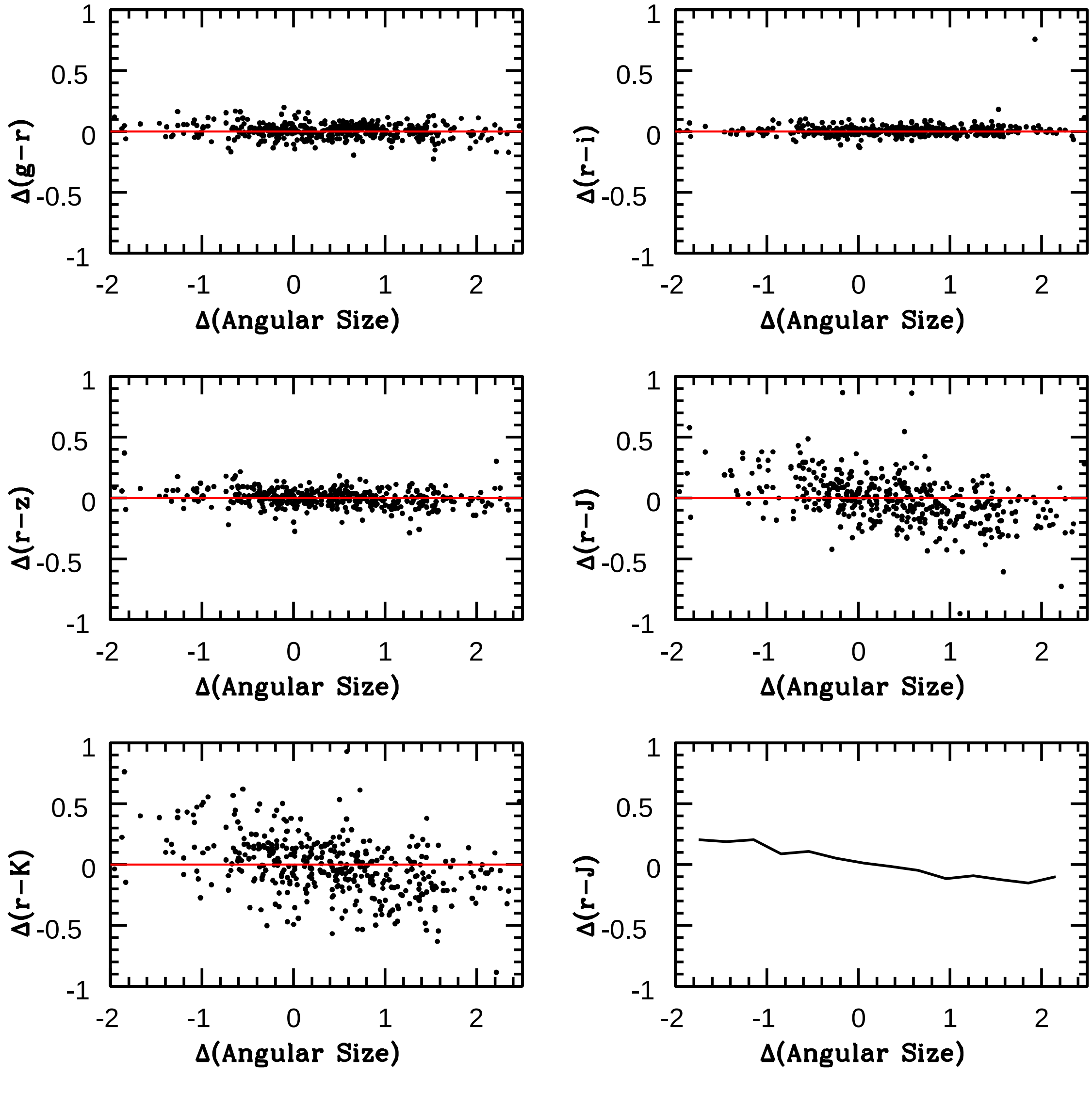

Fig. 6.— The correlation between colour difference and angular size difference for 409 galaxy pairs (see text). The final panel shows the median r-J colour difference as a function of size difference

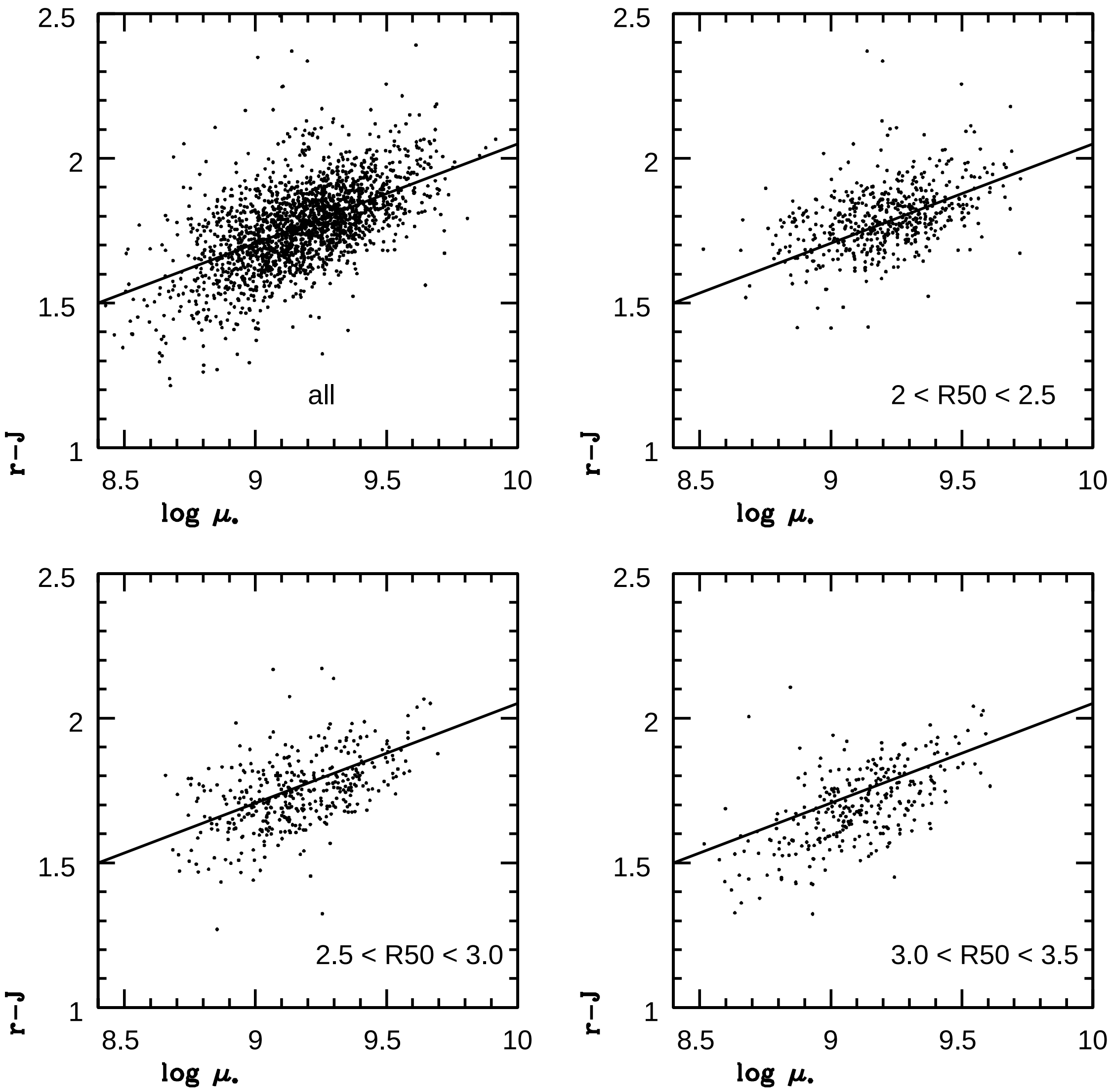

Fig. 7.— The relation between $r-$ colour and stellar surface mass density is plotted for all galaxies and for galaxies in three different ranges of angular size (given as the half-light radius in the z-band in arcseconds).

Table 2: Residuals of the relation between index strengths and velocity dispersion as a function of $g-r$ and $r-J$ colours. Column 2 gives the average S/N ratio of each index, calculated as the ratio between the index strength and the observational error. For each colour, the first and second columns list the slope and mean absolute deviation of the relation fitted with robust technique. The third column indicates the significance of the correlation according to a Spearman rank-order test. Columns 9 and 10 provide some indications about the indices. Column 9 lists the elements that are expected to contribute most to the index strength (in the case of iron, a '+' indicates a weak influence and a '++' a strong influence). Column 10 indicates the sensitivity of the index to α/Fe variations, as expected from Henry & Worthey (1999) and Thomas et al. (2003). Up and down arrows, respectively, correspond to increasing and decreasing index strengths with increasing α/Fe ratio, slanted arrows to intermediate trends, and a hyphen to no sensitivity.

Index	Log(S/N)	$g-r$			$r-J$				
		slope	disp	σ_{corr}	slope	disp	σ_{corr}	element	α/Fe
(1)	(2)	(3)	(4)	(5)	(6)	(7)	(8)	(9)	(10)
CN_1	0.501	0.0381	0.0208	-7.57	0.0090	0.0207	-2.16	C,N	$\uparrow$
CN_2	0.794	0.0107	0.0222	-6.23	0.0062	0.0222	-1.15	C,N	$\uparrow$
Ca4227	0.757	0.0342	0.2084	-5.36	0.0149	0.2084	0.85	Ca,C,N	?
G4300	1.171	0.2666	0.3890	-6.35	0.0346	0.3901	-1.07	C,O,Fe	$\searrow$
Fe4383	1.113	0.6268	0.5053	-5.71	0.1872	0.5059	-2.78	++Fe	$\downarrow$
Ca4455	0.761	0.0450	0.2196	-2.82	0.0322	0.2195	-0.51	Fe,Cr	–
Fe4531	1.000	-0.0845	0.3692	-2.25	0.1099	0.3685	-1.49	+Fe	$\searrow$
C_2	1.169	0.0563	0.6592	-4.69	0.2121	0.6584	-2.78	C,N	$\searrow$
Hβ	0.892	-0.5375	0.2538	8.46	0.0131	0.2557	1.12	–	$\nearrow$
Fe5015	1.137	0.0201	0.4549	0.21	0.0768	0.4548	-0.21	+Fe	$\searrow$
Mg_1	1.240	0.0337	0.0108	-11.38	0.0029	0.0109	-3.33	Mg,C	$\uparrow$
Mg_2	1.470	0.0592	0.0158	-12.42	0.0086	0.0159	-4.50	Mg	$\uparrow$
Mgb	1.199	0.9613	0.3197	-9.73	0.1101	0.3213	-3.91	Mg	$\uparrow$
Fe5270	1.033	0.1583	0.2420	-4.54	0.0633	0.2426	-1.82	++Fe	$\searrow$
Fe5335	0.993	0.0733	0.2625	-3.73	0.0508	0.2627	-2.43	++Fe	$\downarrow$
Fe5406	0.865	0.0394	0.2288	-3.00	0.0667	0.2288	-1.98	++Fe	$\searrow$
Fe5709	0.679	-0.0112	0.1774	-0.36	0.0635	0.1772	-2.08	+Fe	$\searrow$
Fe5782	0.698	0.0806	0.1474	-4.25	0.0924	0.1470	-3.52	+Fe	$\searrow$
NaD	1.291	1.4455	0.4395	-11.15	0.6897	0.4341	-9.61	Na, (ISM)	–
TiO_1	0.758	0.0020	0.0065	-3.73	-0.0005	0.0065	-1.89	O,Ti	–
TiO_2	1.273	0.0068	0.0074	-7.14	0.0034	0.0074	-4.02	O,Ti	–
Hδ	0.389	-2.1096	0.6988	9.37	-0.2406	0.7033	2.23	–	?
Hγ	0.998	-2.2150	0.6672	10.46	0.0492	0.6721	0.43	–	?
$D_n(4000)$	1.950	0.2264	0.0597	-11.89	0.0076	0.0604	-1.91	–	?
[MgFe]′	1.311	0.5345	0.1987	-9.90	0.0982	0.1999	-4.25	Mg,Fe	–
[Mg_1Fe]	1.607	0.0113	0.0149	-5.52	0.0070	0.0149	-2.29	Mg,Fe	–
[Mg_2Fe]	1.662	0.0264	0.0170	-7.64	0.0092	0.0170	-3.06	Mg,Fe	–
$Mg_2/\langle Fe\rangle$	1.115	0.0047	0.0079	-5.93	-0.0004	0.0079	-1.30	Mg,Fe	$\uparrow$

Table 3: Residuals of the relation between index strengths and velocity dispersion as a function of surface stellar mass density, Logμ_*. The first and second columns give respectively the slope and dispersion of the relation fitted with robust technique. The third column indicates the significance of the correlation according to a Spearman rank-order test.

Index	Logμ_*		
	slope	disp	σ_{corr}
CN_1	-0.0016	0.0208	1.69
CN_2	-0.0043	0.0222	2.61
Ca4227	-0.0223	0.2083	1.12
G4300	0.0672	0.3896	-2.22
Fe4383	0.1633	0.5056	-3.07
Ca4455	0.0251	0.2195	-1.66
Fe4531	0.0196	0.3691	-1.92
C_2	0.1343	0.6581	-3.41
Hβ	0.0310	0.2557	-1.23
Fe5015	0.0144	0.4548	-1.52
Mg_1	0.0009	0.0109	-1.63
Mg_2	0.0032	0.0159	-2.55
Mgb	0.1139	0.3209	-4.44
Fe5270	0.0147	0.2427	-2.17
Fe5335	0.0529	0.2626	-2.88
Fe5406	0.0038	0.2290	-2.26
Fe5709	0.0175	0.1772	-0.86
Fe5782	0.0384	0.1474	-2.19
NaD	0.1533	0.4418	-5.70
TiO_1	0.0021	0.0065	-4.15
TiO_2	0.0021	0.0074	-3.45
Hδ	-0.0176	0.7039	0.54
Hγ	-0.0450	0.6722	0.32
$D_n(4000)$	-0.0155	0.0604	1.93
$[MgFe]'$	0.0572	0.2001	-5.48
$[Mg_1Fe]$	0.0014	0.0149	-2.51
$[Mg_2Fe]$	0.0043	0.0170	-3.20
$Mg_2/\langle Fe\rangle$	-0.0006	0.0079	1.74